Bull Mater Sci (2020)43:197
https://doi.org/10.1007/s12034-020-02164-w

Electrical, thermal and elastic properties of methylammonium lead bromide single crystal

R MUKHERJEE
Department of Physics, School of Chemical Engineering and Physical Science, Lovely Professional University, Jalandhar 144411, India
rupam.23644@lpu.co.in

MS received 25 December 2019; accepted 14 May 2020

Abstract. We report temperature-dependent dielectric permittivity, thermal conductivity and mechanical resonances of as-grown hybrid perovskite single crystal $CH_3NH_3PbBr_3$. Structural phase transitions are analysed using new experimental techniques, where thermal conductivity by steady-state process and elastic modulai by ultra-resonance spectroscopy is carried out through [100] and [110] directions, respectively. Performing thermal conductivity measurement on small-sized samples usually pose a significant challenge due to its dimensional limit. Following the steady-state technique, we measured the thermal conductivity of around 1 W m^{-1} K^{-1} in the temperature range 100–300 K on 2 × 2 mm^2 size crystal. This is found to be comparable with I^{+3} anion-based hybrid perovskites as reported by Pisoni *et al* 2014 *J. Phys. Chem. Lett.* **5** 2488. Room temperature electrical resistivity and dielectric permittivity of order 10^9 and 10^2, respectively, shows sharp transitions while approaching 150 K, which strongly supports first-order structural transition. Thermally activated resistivity behaviour above 280 K follows $1/T$ dependence, yielding activation energy of 0.2 eV. Softening of elastic moduli on approaching the phase transition is analysed from resonant ultrasound spectroscopy measurement. Square of the resonance frequency is found to diverge below 236 K, which inhibits any further experimental determination of elastic moduli at low temperature.

Keywords. Hybrid perovskites; thermal conductivity; resonance; steady state.

1. Introduction

Perovskite with crystal structure ABO_3 has proved to have wide range of optical and transport properties, depending on the choice of occupation of basis at A and B sites [1,2]. Recently hybrid organic–inorganic materials with chemical unit $CH_3NH_3PbX_3$ (X = Cl, Br, I) are gaining fast attention, in which A-site is occupied by an organic methylamine (MA) cation and B-site by an inorganic cation. This class of materials display large scale of electronic and photoconductive properties, which is mainly due to the existence of both covalent and Van der Waals bond within a unit cell [3–5]. Hybrid perovskite $MAPbI_3$ has already successfully achieved high conversion efficiency (21%) for solid-state sensitized solar cell device [6]. The additional merits of using $MAPbI_3$ in solar cell devices are its high carrier mobility (1–175 μm), low thermal conductivity (0.5 W m^{-1} K^{-1} at 300 K) and easily tunable electrical properties *via* photo-induced or chemical doping [7–9]. This also opens up new opportunities for developing flexible power generation paving the path for green technology. However, this iodide-based hybrid perovskite suffers a major drawback due to its chemical and thermal instability at wide range of temperature range [10,11]. Moreover due to the presence of spin-orbit coupling in $MAPbI_3$, it shows ambipolar-type carrier conduction, which is detrimental for device application [12,13]. Another class of organic–inorganic perovskite material is $CH_3NH_3PbBr_3$ ($MAPbBr_3$), where iodine is replaced by bromine forming $PbBr_6$ octahedral [14,15]. $MAPbBr_3$ shows cubic structure at room temperature and is considered to be more thermodynamically stable under certain atmospheric conditions [16]. However, much of its physical properties in ambient conditions are still unknown. More experimental measurements are required to study the fundamental properties and thereafter to understand the relation between structural fluctuation and electronic structure.

In this article, we report the detailed studies of electrical properties, lattice thermal conductivity and elastic properties on $MAPbBr_3$ single crystal in the temperature range, which includes three different structural phases. A low thermal conductivity 1 W m^{-1} K^{-1} at room temperature is observed, which is assumed to be due to strong phonon scattering by thermally activated rotating molecules. The low magnitude of thermal conductivity in $MAPbBr_3$ opens up a new path to grow promising thermoelectric materials in most inexpensive and effortless way. A dip in lattice thermal conductivity is observed at phase transition

Published online: 12 August 2020

temperatures 151 and 236 K. At 151 K, the structural transition is accompanied by sharp rise in dielectric permittivity with no peak in dielectric loss. Maximum dielectric permittivity of 175 with loss less than 0.1 at 30 KHz is found to be very promising and can also possibly considered to be a good dielectric candidate. This phenomenon has further urged us to investigate localized vibrational modes by measuring the free-body resonance of the sample. For the first time, resonant ultrasound spectroscopy (RUS) technique is used on $MAPbBr_3$ sample, which is a nondestructive method of determining a material's elastic response based on the measurement of the resonances of a freely vibrating body [17,18]. In our experiment, it is found that elastic moduli in $MAPbBr_3$ grows soft on lowering down the temperature and diverges at structural phase transition. This observation agrees well with the electrical and thermal response, which further confirms the presence of multiple structural transitions in $MAPbBr_3$ crystals. Each of the measuring techniques thus adds up a new dimension to study the phase transitions and the associated properties simultaneously and more precisely.

2. Experimental

Solution-grown single crystals of $MAPbBr_3$ with flat facets of 2×2 mm^2 and thickness of 1 mm were used for our study. One molar solution of $PbBr_2$ (Alfa Aesar, 99.999%) and MABr (Aldrich, 98%) was prepared in 10 ml dimethylformamide. All reagents were used as-received without further purification. The solution was prepared in a vial which was then kept in an oil bath undisturbed at 80°C. Bright orange crystals nucleated in 1 h. Crystals were then placed under vacuum to remove the solvent. All procedures were conducted in open air under ambient conditions. The complex dielectric permittivity and a.c. conductivity were measured using a precision LCR meter (Agilent 4282A) at temperatures between 100 and 380 K and at frequencies between 20 Hz to 2 MHz. Oscillating voltage of 1 V was applied throughout the dielectric measurement. Resistivity and thermal conductivity measurement was performed in close cycle refrigerator (CCR) form ARS. The elastic moduli were determined using RUS and a custom-made probe in Quantum design Versa lab cryostat. Sample excitation and data collection were executed by Stanford Research synthesized function generator and model SR 844 lock-in amplifier.

3. Results and discussion

3.1 *Material characterization*

Phase purity was examined with powder X-ray diffraction (XRD) on pulverized crystals of $MAPbBr_3$, at room temperature with Rigaku X-ray diffractometer in the 2θ range 15–100°. The observed powder XRD pattern, as shown in figure 1, was refined with Rietveld method. The refinement confirms that the as-grown crystals are in single phase with cubic structure (space group *Pm3m*). The inset shows an image of the bright orange colour single crystal.

3.2 *Electrical characterization*

Temperature-dependent resistivity (ρ) of bulk $MAPbBr_3$ single crystal is plotted in a log-linear scale as shown in figure 2. The resistivity (ρ) at room temperature is found to be $0.2 \times 109\ \Omega$ cm, which increases by an order of magnitude around 145 K. Resistivity at the structural transition temperatures 236 and 151 K shows a kink as shown by the arrows in the figure. In the region $T < 150$ K, resistivity rises sharply with decreasing temperature, while for $151 < T < 240$ K, resistivity shows a weak temperature-dependence behaviour followed by region $T > 240$ K, where it follows an ideal semiconductor behaviour. The weak temperature response shows the presence of hopping type conduction due to existence of charge trap carriers. Resistivity around room temperature shows thermally activated behaviour, which is given as $\rho = A \exp(E_a/K_B T)$, where A is a pre-exponential term, E_a is an activation energy, K_B is the Boltzmann's constant and T the temperature in Kelvin. The inset of figure 2 shows the Arrhenius fitting (red line) in the semi-log plot within the temperature range 285–310 K. E_a is found to be 0.2 eV, which lies well within the class of semiconductor bandgap. Organic–inorganic perovskites have both ionic and electronic charge carriers, which have different temperature differences due to its respective effective mass [19,20]. To shed additional light on the transport mechanism and relaxation mechanism, impedance spectroscopy has been used to study the temperature-dependent ac conductivity and dielectric response. As shown in figure 3a, the real part of complex permittivity (ε')

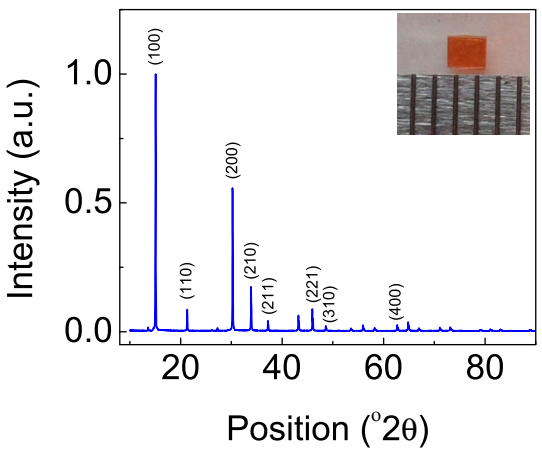

Figure 1. The powder X-ray diffraction of $MAPbBr_3$ at room temperature. The inset displays the image of bright orange $MAPbBr_3$ single crystal.

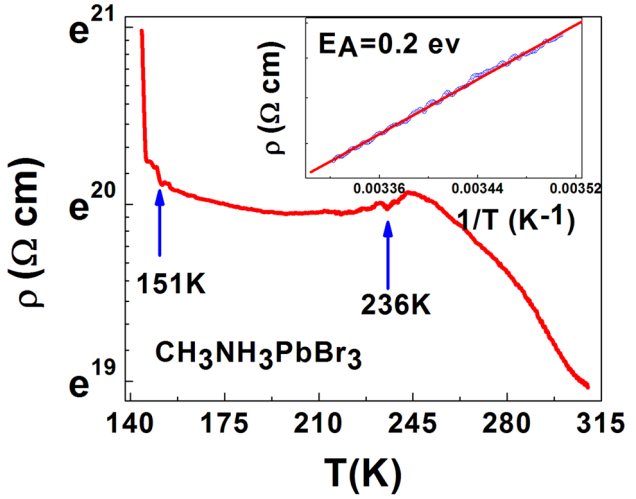

Figure 2. Resistivity as a function of temperature for $CH_3NH_3PbBr_3$ single crystal. Three distinct regions of conduction are observed. Transitions are observed as shown by the arrow at 151 and 236 K. The inset shows linear behaviour of resistivity as a function of inverse temperature in log-linear plot.

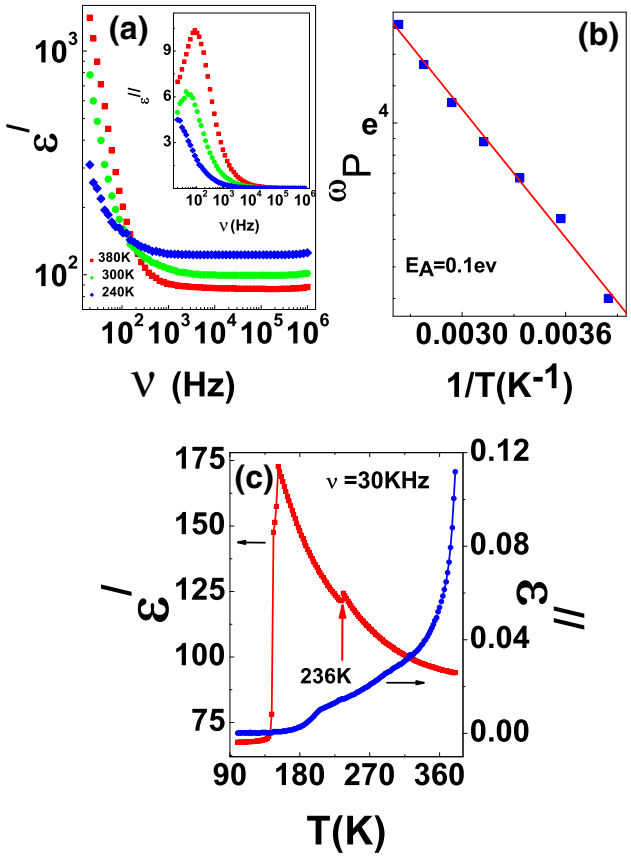

Figure 3. (**a**) Frequency dependent real part of permittivity (ε') at 380, 300 and 240 K is shown. The inset shows imaginary part (ε'') as a function of frequency. Relaxation peaks are observed at low frequency. (**b**) ln-linear plot shows Arrhenius fitting with relaxation peak frequency as function of inverse of temperature. Activation energy is determined from the slope. (c) Temperature-dependent ε' and ε'' at oscillating frequency of 30 KHz is shown. Discontinuities at 151 and 236 K in real part of permittivity are clearly observed.

for frequencies $\nu > 200$ Hz decreases as temperature increases. Whereas for $\nu < 200$ Hz, s' increased by an order of magnitude up to 1400 at 20 Hz and 380 K followed by a peak in dielectric loss (ε'') as shown in the inset.

To our knowledge no data for dielectric permittivity on single crystal of $MAPbBr_3$ is reported. However, investigation by other groups on powdered crystals showed much lower value of temperature-dependent dielectric permittivity at 1 KHz [21]. These high values of ε' and ε'' at low frequencies found to decrease with decreasing temperature. Figure 3b shows the Arrhenius temperature dependence of loss peak frequency (ω_P), which is related as $\omega_P \exp(-W/K_BT)$, where W is an activation energy. In the temperature range 380–260 K, Arrhenius-type behaviour is obeyed yielding W as 0.1 eV, which is a characteristics of Debye-type relaxation. But for $T < 260$ K, Arrhenius-type behaviour is not observed as the peak in ε'' disappears at low frequency, which strongly indicates the presence of slow moving hopping charge carriers with different relaxation behaviour. Figure 3c represents temperature dependence of real part (ε') and imaginary part (ε'') of complex permittivity at frequency 30 KHz within temperature range 380–100 K. Two distinct frequency independent peaks, a small peak at 236 K and a sharp peak at 151 K are observed. At 151 K, the sharp decrease of ε' from 172 to 65 reflects first-order structural phase transition from tetragonal to orthorhombic, which has induced long-range orientational order of dipole moments. In addition for $T > 151$ K, ε' is seen to decrease continuously with increase in temperature, further following the para-electric behaviour. Moreover, from figure 3c both real part and the imaginary part of dielectric permittivity, which is around 67 and 10^{-3}, is found to be independent of temperatures below 135 and 160 K, respectively.

3.3 *Thermal characterization*

In figure 4, lattice thermal conductivity (κ_L) of single crystal $MAPbBr_3$ is shown at temperature (T) range 5–300 K. According to Debye model, the lattice contribution to thermal conductivity is described as

$$\kappa_L \propto T^3 \int_0^{\theta_D/T} x^4 e^x \Big/ (e^x - 1)^2 \tau(\omega, T) dx$$

where $x = (h\omega/2\pi K_BT)$, θ_D is the Debye temperature and τ the relaxation time of a phonon. Ultra low value of $\kappa_L \approx 0.6$ W m^{-1} K^{-1} at 300 K, which increases to 2.5 W m^{-1} K^{-1} at 13 K. Moreover in figure 4, kinks are observed in κ_L at around 236 and 150 K, which is mainly associated with structural phase transition as confirmed from dielectric measurements. With respect to the thermal conductivity of $MAPbI_3$ perovskite single crystal, the magnitude of κ_L in $MAPbBr_3$ is found to be comparable at room temperature. The same order of magnitude of κ_L at room temperature

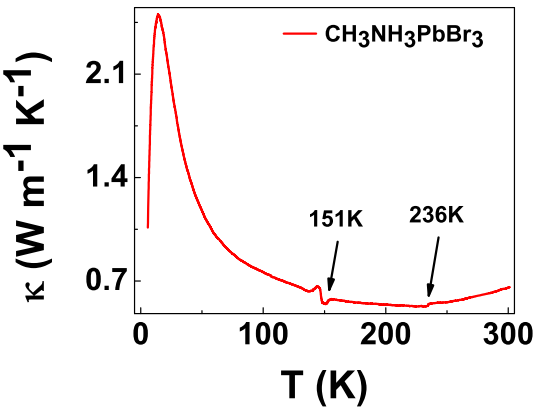

Figure 4. Thermal conductivity on single crystal of $CH_3NH_3PbBr_3$ is shown here. At structural transitions 151 and 236 K discontinuities are observed.

irrespective of bromine or iodine cations reflects the fact that lifetime of acoustic phonon is short and phonon mean-free path is comparable to lattice parameters. Referring to figure 4, for $T > 236$ K approaching from tetragonal to cubic phase κ_L is found to increase, which implies weakening effect of phonon–phonon scattering due to much longer optical phonon lifetime. This phenomenon can be explained by the fact that in cubic phase the gap between optical mode and acoustic mode is bigger compare to gap in tetragonal phase [22]. This results in less scattering or increased phonon lifetime in cubic phase. But the reason behind ultra-low value of κ_L at high temperature is probably due to the fact that MA molecules acting as a 'rattler' has an additional degrees of freedom, which can interfere with conduction phonons. This leads to lower phonon group velocity and strong anharmonicity rising from thermally disordered rotating MA cation and thus inhibiting the flow of phonon energy. Temperature-dependent thermal conductivity below 14 K is found to be proportional to T3, which agrees well with Debye model.

From Wiedemann–Franz law, contribution from the electronic part (κ_e) is found to be less than 9×10^{-6} μW m^{-1} K^{-1}, which can be neglected throughout our temperature range domain. This strongly suggests that thermal conductivity in $MAPbBr_3$ is mainly lattice phenomenon.

3.4 *Elastic characterization*

For single crystals, determination of the full elastic tensor typically requires that samples are shaped into rectangular parallelopipeds with faces perpendicular to the main crystallographic directions. Unfortunately, the brittle nature of the $MAPbBr_3$ crystals prevents the crystals from being cut into the desired shape without causing multiple cracks and fractures. However, the squared resonant frequencies are directly proportional to the elastic moduli, and tracking the temperature dependence of the resonances allows us to address the temperature dependence of the elastic moduli. Using a custom-built probe that was inserted into a Quantum Design Versa-Lab system, we collected data on five resonant frequencies as a function of temperature.

Figure 5 shows the temperature-dependent behaviour of the resonant frequencies for $MAPbBr_3$. The data shown in figure 5 deviate from the 'typical' behaviour observed in solids that do not display any thermodynamic irregularities, i.e., a gradual stiffening with decreasing temperature, or the so-called Varshni function [23]. The elastic moduli soften with decreasing temperature, reaching a minimum at approximately 236 K that coincides with the structural transition seen in the transport measurements. Below 236 K, the resonant frequencies cannot be determined due to the excessive attenuation that accompanies the phase transition.

4. Conclusion

In conclusion, we have synthesized single crystal of $MAPbBr_3$ of regular cubic shape. Electrical measurements show complex conduction mechanisms at different ranges of temperature. Structural transitions at 236 and 151 K are confirmed from electrical, thermal and elastic measurements. Low thermal conductivity in $MAPbBr_3$ crystal is mainly attributed to organic MA cation, which acts as a rattler atom and has rotational degree of freedom that strongly scatters the energetic phonons. Dielectric measurement clearly depicts the temperature at which rotation of MA ion freezes, which is followed by dramatic change in dielectric permittivity. RUS measurements too have confirmed the multiple structural transitions and have shown softening of elastic modes at phase transition temperatures, as approached from higher temperature.

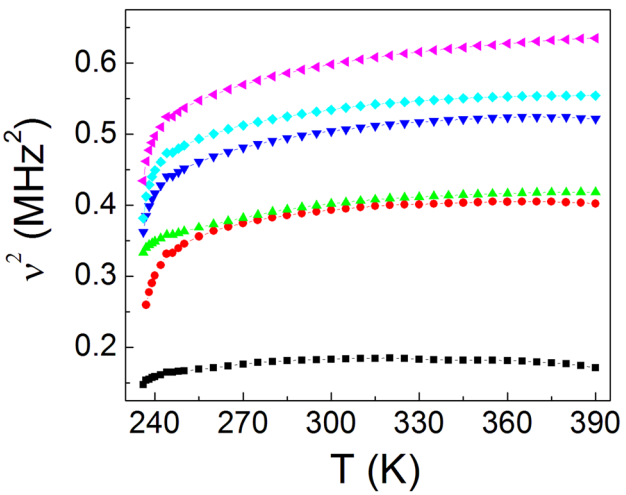

Figure 5. Square of resonant frequencies as a function of temperature is shown. Softening of elastic modes is seen with lowering of temperature.

References

[1] Liang J, Liu J and Jin Z 2017 *Sol. RRL* **1** 1700086
[2] Dong Q, Lei L, Mendes J and So F 2020 *J. Phys. Mater.* **3** 012002
[3] Mitzi D B 2000 *Inorg. Chem.* **39** 6107
[4] Zhu X, Lin Y, Martin J S, Sun Y, Zhu D and Yan Y 2019 *Nat. Commun.* **10** 2843
[5] Chang C Y, Solodukhin A N, Liao S Y, Mahesh K P O, Hsu C L, Ponomarenko S A *et al* 2019 *J. Mater. Chem. C* **7** 8634
[6] Chen Z 2019 *ACS Energy Lett.* **4** 1258
[7] Herz L M 2017 *ACS Energy Lett.* **2** 1539
[8] Frolova L A, Dremova N N and Troshin P A 2015 *Chem. Commun.* **51** 14917
[9] Pisoni A, Jaćimović J, Barišić O S, Spina M, Gaál R, Forró L *et al* 2014 *J. Phys. Chem. Lett.* **5** 2488
[10] Kumar V, Barbé J, Schmidt W L, Tsevas K, Ozkan B, Handley C M *et al* 2018 *J. Mater. Chem. A* **6** 23578
[11] Zhou Y and Zhao Y 2019 *Energy Environ. Sci.* **12** 1495
[12] Giorgi G and Yamashita K 2015 *J. Mater. Chem. A* **3** 8981
[13] Senanayak S P, Yang B, Thomas T H, Giesbrecht N, Huang W, Gann E *et al* 2017 *Sci. Adv*. **3** 1
[14] Wang K H, Li L C, Shellaiah M and Sun K W 2017 *Sci. Rep.* **7** 13643
[15] Jeon N J, Noh J H, Yang W S, Kim Y C, Ryu S, Seo J *et al* 2015 *Nature* **517** 476
[16] Wang C, Ecker B R, Wei H, Huang J and Gao Y 2018 *J. Phys. Chem. C* **122** 3513
[17] Migliori A and Maynard J D 2005 *Rev. Sci. Instrum.* **76** 121301
[18] Migliori A 1993 *Physica B*: *Condens. Matter* **183** 1
[19] Galkowski K, Mitioglu A, Miyata A, Plochocka P, Portugall O, Eperon G E *et al* 2016 *Energy Environ. Sci*. **9** 962
[20] Parker A G, Gehring P M, Skelton J M, Smith I C, Parshall D, Frost J M *et al* 2018 *Proc. Natl. Acad. Sci.* **115** 11905
[21] Yamamuro N O, Matsuo T and Suga H 1991 *J. Chem. Thermodyn.* **23** 987
[22] Sendner M, Nayak P K, Egger D A, Beck S, Muller C, Epding B *et al* 2016 *Mater. Horiz.* **3** 613
[23] Keppens V, Mandrus D, Sales B C, Chakoumakos B C, Dai P, Coldea R *et al* 1998 *Nature* **395** 876